PNAS RESEARCH ARTICLE | EARTH, ATMOSPHERIC, AND PLANETARY SCIENCES

# Miocene surface uplift and orogenic evolution of the southern Andean Plateau (central Puna), northwestern Argentina

Heiko Pingel[a,1], Ricardo N. Alonso[b], Bodo Bookhagen[a], John M. Cottle[c], Andreas Mulch[d,e], Alexander Rohrmann[a,f], and Manfred R. Strecker[a]

Edited by Victor Ramos, Universidad de Buenos Aires, Buenos Aires, Argentina; received March 23, 2023; accepted September 5, 2023

**We present stable hydrogen-isotope analyses of volcanic glass (δDg) and radiometric ages (U–Pb zircon, U–Th calcite, AMS $^{14}$C) from deformed sedimentary deposits in the vicinity of the intermontane Pocitos Basin in the central Puna of the Andean Plateau at about 24.5°S. Our results demonstrate 2-km surface uplift since the middle to late Miocene and protracted shortening that persists until the present day, while other sectors of the Puna show evidence for tectonically neutral and/or extensional settings. These findings are at odds with previous studies suggesting near-modern elevations (4 km) of the Puna Plateau since the late Eocene and formation of the intermontane Miocene Arizaro-Pocitos Basin associated with gravitational foundering of a dense lithosphere. Geophysical and geochemical data support the removal of continental lithosphere beneath the Puna, but the timing and mechanisms by which this removal occurs have remained controversial. We hypothesize that intermontane basin formation in the central Puna is the result of crustal shortening since about 20 Ma, followed by rapid surface uplift, likely related to lithospheric delamination.**

Central Andes | Puna Plateau | NW Argentina | tectonics | stable isotope paleoaltimetry

## Significance

The uplift of the Puna Plateau in the South-Central Andes of NW Argentina has long been puzzling. Previous estimates for when the plateau reached its current height have varied widely, from 40 to 10 million years ago (Mya), making it difficult to understand the forces that shaped its unique features. Our research, using stable isotope-based paleoelevation estimates from hydrated volcanic glass, shows that the plateau rose rapidly from 2 to 4 km between 13 and 10 Mya. We also present evidence of ongoing deformation since the middle Miocene. These findings shed light on the geological processes in the Central Andes, which may improve our understanding of the relative roles of mantle and crustal dynamics in shaping the plateau topography.

The high-elevation, intraorogenic Andean Plateau (Altiplano-Puna) is a first-order morphotectonic province of the Central Andes and constitutes the world's second-largest orogenic plateau with an average elevation of 4 km, e.g., ref. 1 and Fig. 1*A*. Its formation is attributed to the subduction of the Nazca Plate beneath the South American continent and associated mantle processes, which has caused significant crustal deformation in the overriding plate since the Eo–Oligocene, e.g., refs. 1 and 2. However, there is considerable debate regarding the timing and style of plateau uplift, which remains one of the most controversial issues in the late Cenozoic evolution of the Andes. Among the most discussed models are a) shortening and crustal thickening (1); b) lithospheric foundering (3–5); c) systematic eastward orogenic growth e.g., ref. 6; d) broken-foreland evolution, e.g., ref. 7; and e) changes in convergence direction, velocity, and slab geometry of the subducting Nazca plate and the overriding South American plate, e.g., ref. 8.

Evidence for lithospheric foundering beneath the southern Andean Plateau (Puna Plateau) comes, for example, from a series of geophysical studies documenting a relatively thin crust (50 to 55 km) and a thinned or absent lithospheric mantle that has been replaced by hot and buoyant asthenosphere, e.g., refs. 9–16. However, the style and timing of this lithospheric removal remain debated. Two principal scenarios are being discussed for the central and southern Puna: a) delamination of the lower lithosphere as a coherent slab (17, 18) and b) Rayleigh–Taylor instabilities (RT-drip) causing dense lithosphere to descend into the asthenosphere (19–21).

In this context, the study of sedimentary basins in the plateau realm can provide valuable insights into the late Cenozoic evolution of the Andes and help elucidate the underlying hypotheses by revealing the relationships between tectonic deformation and surface uplift in response to geodynamic processes. While there are many unifying sedimentary basin characteristics along strike of the Andean Plateau, including internal drainage, semiarid to arid climate and associated deposition of evaporites, there are notable differences between the northern and southern sectors of the plateau. In contrast to the extensive basins of the Altiplano in the north with a mean elevation of 3.8 km, and incipient establishment of fluvial connectivity and sediment transport to the foreland, the Argentine Puna to the south has a mean elevation of 4.4 km and comprises numerous smaller basins bordered by reverse-fault bounded ranges up to 6 km high. The Puna is internally drained and fluvially disconnected from the foreland, resulting in thick sedimentary basin fills that include continental evaporites and volcanic and clastic deposits, typically between 3 and 5 km thick, e.g., refs. 1, 22, and 23.

Author contributions: H.P., B.B., A.M., and M.R.S. designed research; H.P., R.N.A., B.B., J.M.C., A.M., A.R., and M.R.S. performed research; J.M.C. and A.M. analyzed data; and H.P., R.N.A., B.B., J.M.C., A.M., A.R., and M.R.S. wrote the paper.

The authors declare no competing interest.

This article is a PNAS Direct Submission.



[1]To whom correspondence may be addressed. Email: heiko.pingel@geo.uni-potsdam.de.

This article contains supporting information online at https://www.pnas.org/lookup/suppl/doi:10.1073/pnas.2303964120/-/DCSupplemental.

Published October 9, 2023.

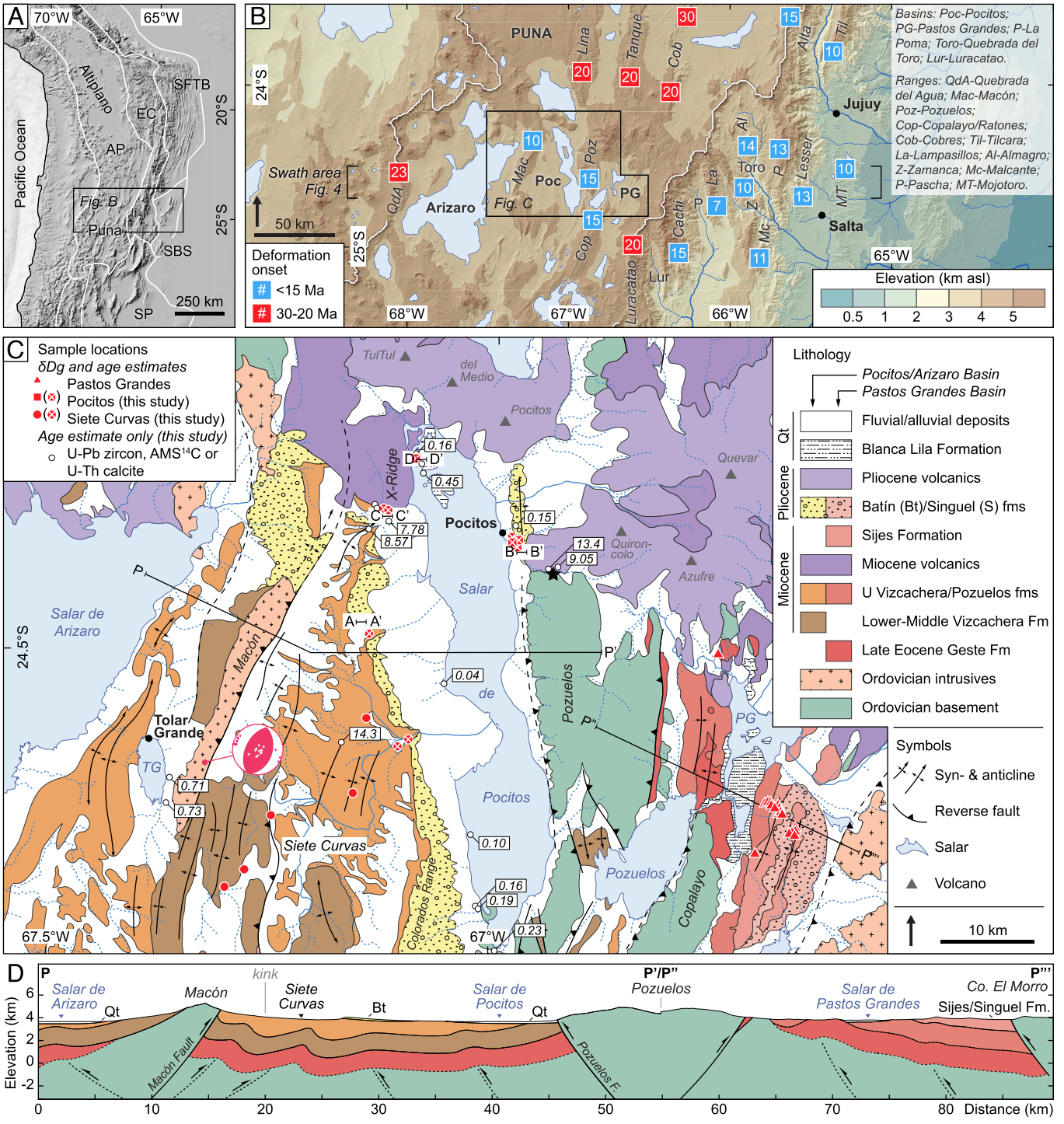


**Fig. 1.** Overview maps and cross-section of the study area in the central Puna Plateau. (*A*) Shaded relief map showing morphotectonic provinces of the Central Andes. AP, Andean Plateau; EC, Eastern Cordillera; SFTB, Subandean fold-and-thrust belt; SBS, Santa Bárbara System; SP, Sierras Pampeanas. (*B*) Topographic map of the southern Central Andes showing major basins and ranges discussed in the text. Numbered squares indicate age of deformation onset and range uplift in Ma compiled from the literature (e.g., refs. 24–26, for a complete list see *SI Appendix*, Table S2). The white line delineates watershed between the internally drained Puna Plateau and adjacent provinces. (*C*) Geological map of the Salar de Pocitos basin and adjacent regions (Arizaro, Siete Curvas, and Pastos Grandes) modified after Alonso (27), Blasco et al. (28), DeCelles et al. (21), and Martínez et al. (29). PG, Salar de Pastos Grandes; TG, Salina Tolar Grande. Shown are a) a pseudo-fault-plane solution calculated from fault-kinematic indicators documenting thrust kinematics of the Macón Fault (*SI Appendix*, Table S3) and b) δDg and geochronologic sample locations with selected age estimates as listed in Table 1 and *SI Appendix*, Table S13. Black lines show the location of cross-sections shown in *D* and Fig. 3. The black star shows the location of the Quebrada Quirón site discussed in the text. (*D*) Schematic geologic cross-section (P'–P"' in *C*) through the study area (modified after 21, 30). Bt, Batín Formation; Qt, Quaternary fill.

Stable isotope paleoaltimetry permits assessment of tectonically controlled surface-elevation changes through time, e.g., refs. 5 and 31–42, and the results of these studies have propelled ample discussions about the timing, causes, and consequences of surface uplift, especially of the Andean Plateau and its neighboring provinces, e.g., refs. 43 and 44. Stable isotope paleoaltimetry utilizes the systematic depletion of heavy isotopes in precipitation ($^{18}O$ and $^{2}H$) with increasing altitude at which precipitation

occurs (45). Oxygen and/or hydrogen isotope ratios of meteoric water preserved in ancient proxy materials such as soil carbonates, clay and mica minerals, organic biomarkers, or volcanic glass shards can thus aid in topographic reconstructions, e.g., refs. 32 and 46–49. If available, volcanic glass from tuffs and ignimbrites has many advantages as a proxy material for stable isotope analysis: a) Volcanic glass assimilates up to 5 to 10 wt% water from the environment after deposition; b) saturation is reached after about 5 to 10 kyr, after which no significant hydrogen isotope exchange occurs, e.g., refs. 46 and 50; and c) its depositional age can be reasonably well determined by radiometric dating of associated minerals, eliminating the need for continuous sediment records with sporadic age constraints, e.g., ref. 39. This and its abundance in sedimentary sequences of the Puna and the basins of the Eastern Cordillera make hydrated volcanic glass a perfect proxy material for spatiotemporal paleoaltimetry studies in this region.

We report 26 U–Pb zircon ages and hydrogen isotopic compositions of hydrated volcanic glass ($\delta$Dg) from 10 tuffs intercalated with deformed Mio–Pleistocene basin strata in the vicinity of the intermontane Pocitos Basin (ca. 3.6 km asl) with the ultimate goal of deciphering the surface uplift history and tectono-sedimentary evolution in the central Puna Plateau at ca. 24.5°S. Combined with existing data, our results support protracted shortening in this sector of the plateau since 20 Ma and rapid, kilometer-scale surface uplift between 13 and 10 Ma, possibly related to middle Miocene crustal thickening and subsequent lithospheric delamination. This scenario is an alternative to previous models predicting near-modern paleoelevations for the southern and central Puna since the Eocene (33), and the enigmatic formation of hinterland basins related to RT-drip formation beneath the neighboring Miocene Arizaro Basin (21).

## Geological Setting

The Puna of northwestern Argentina is a largely internally drained morphotectonic province of the Andean Plateau bordered to the West and East by an active volcanic arc and the Eastern Cordillera thick-skinned thrust belt, respectively (Fig. 1 *A* and *B*). The Puna's compressional basin-and-range morphology includes many extensive sedimentary basins that are separated from each other by reverse-fault bounded mountain ranges and volcanic edifices, (e.g., ref. 22). Between about 24 and 25°S, these basins include, from West to East, the Arizaro, Pocitos, and Pastos Grandes basins (Fig. 1 *B* and *C*), in which limited runoff conditions and an arid climate with annual rainfall of <100 to 200 mm have led to the formation of large playas and associated alluvial fans.

The N–S-oriented Pocitos Basin is a vestige of a formerly contiguous sedimentary basin (including the Arizaro Basin to the west) in the interior of the Puna that was partitioned during Miocene contractional deformation, e.g., refs. 21 and 30. To the West, the Pocitos Basin is bordered by the E-dipping limb of an N–S-oriented anticline in Neogene sedimentary rocks. This structure forms the Colorados Range (Fig. 1*C*) and separates the basin from Siete Curvas, a region characterized by outcrops of strongly folded and faulted redbeds of the Miocene Vizcachera Formation (e.g., refs. 21 and 30). This region is in turn bordered to the west by the Macón Range, which has been uplifted along a west-dipping reverse fault at 10 ± 5 Ma (21, 51). To the east, the Pocitos Basin is bordered by the reverse-fault bounded Pozuelos and Copalayo ranges, which separate it from the adjacent Pozuelos and Pastos Grandes basins to the east. The northern extent of all these basins is delimited by transverse Mio-Pliocene volcanic centers (TuMePo-El Quevar magmatic belt) along the Calama–Olacapato–El Toro lineament, e.g., refs. 17 and 52.

The regional basement is composed of low-grade marine metasediments of the Ordovician Copalayo Formation, e.g., at the Pozuelos and Copalayo ranges, (53) and Ordovician igneous rocks, e.g., at the Macón Range, 483–474 Ma, (54, 55). Initial deformation and low-grade metamorphism of these basement rocks are, in general, attributed to the Oclóyic orogeny at the end of the Ordovician, (e.g., ref. 56). In addition, multiproxy thermochronological investigations have shown that the Ordovician basement of the western and east-central Puna has resided at temperatures below 200 °C (<6 km) since the Devonian and early Cretaceous, respectively (55), and modeling of detrital AFT and (U–Th)/He ages indicates monotonic local source-terrane cooling during the early-middle Cretaceous, followed by relatively rapid Eocene cooling (21, 51).

In the adjacent Arizaro and Pastos Grandes basins, these Paleozoic basement rocks are unconformably overlain by the middle to late Eocene Geste Formation, e.g., refs. 27 and 57—a more than 2-km-thick coarsening-upward sequence of regionally widespread continental redbeds, e.g., refs. 58–63, associated with the Eocene foreland basin located in the present-day Puna and Eastern Cordillera provinces of northwest Argentina, e.g., ref. 64. No outcrops of the Geste Formation have been detected in the Pocitos area, but its presence in the subsurface cannot be excluded (30). At Siete Curvas, the basement is unconformably overlain by a more than 3-km-thick sequence of Neogene clastic deposits (ca. 24–8 Ma) that have been grouped into the Vizcachera Formation (21, 22, 28, 65). Additional outcrops of this unit may be located southeast of the Salar de Pocitos, overlying the Ordovician basement of the Pozuelos Range Fig. 1*C*, e.g., ref. 29, along the western flanks of the Macón Range (30), and at the southwestern margin of the Arizaro Basin (21), suggesting a continuation of the Vizcachera Formation in the subsurface of the Arizaro and Pocitos basins (Fig. 1*D*).

In the Pastos Grandes Basin, along the northeastern flank of the Copalayo Range, the Geste Formation is overlain by the poorly dated, halite-bearing Pozuelos Formation [>8 Ma, (22, 41)]. The basal age of the Pozuelos Formation may be inferred from stratigraphic correlation with tilted strata of the Catal Formation along the eastern flanks of the Ratones Range Sierra de Bequeville in ref. 66, which is the southern continuation of the Copalayo Range. Here, the Geste Formation is unconformably overlain by volcaniclastic (16.7 ± 0.1 Ma, Ar/Ar) and conglomeratic (13.2 ± 0.3 Ma, Ar/Ar) strata whose tectonosedimentary relationships suggest syntectonic deposition (66). The Pozuelos Formation is unconformably overlain by interbedded sequences of borates and gypsiferous mud and siltstones of the Sijes Formation (ca. 8–6 Ma), the conglomeratic Singuel Formation (ca. 6–2.5), and the Pleistocene Blanca Lila Formation (41, 67).

In the Pocitos Basin, the Miocene Vizcachera Formation is unconformably overlain by the Mio–Pliocene conglomeratic Batín Formation (68). Finally, the evaporitic Blanca Lila Formation was deposited during the Pleistocene (67, 69).

## Results

**Geochronology.** U–Pb zircon geochronology of volcanic ashes and ignimbrites collected from outcrops in the Pocitos and Arizaro basins and at Siete Curvas yielded ages ranging from ca. 14 to <1 Ma (Table 1 and *SI Appendix*, Figs. S1 and S2). U–Th calcite dating of a stromatolitic layer of the Blanca Lila Formation yielded a mean age of 0.45 ± 0.03 Ma. Finally, AMS$^{14}$C dating of a terrace-capping, pisolithic calcrete on the western shore of Salar de Pocitos yielded an age of 40,180 (+1420/–1200) y

**Table 1. Summary of new-age constraints and hydrogen isotope data**

| Sample ID | Lat (°) | Long (°) | z (m asl) | Age ± 2σ (Ma) | Method | MSWD | Grains* | Individual δDg (‰) I | II | III | Mean δDg‡ ± 2σ (‰) | Mean $H_2O$§ ± 2σ (wt%) | Additional information |
|---|---|---|---|---|---|---|---|---|---|---|---|---|---|
| KIA48048 | −24.527 | −67.057 | 3670 | 0.044 ± 0.002 | AMS $^{14}$C (cal BP) | – | – | – | – | – | – | – | Calcrete |
| SP080314-2 | −24.675 | −67.025 | 3660 | 0.10 ± 0.01 | U–Pb zircon | – | 2/49† | – | – | – | – | – | Tuff, playa/lacustrine |
| SP160316-3 | −24.371 | −66.971 | 3732 | 0.15 ± 0.03 | U–Pb zircon | 2.13 | 4/40 | – | – | – | – | – | Tuff, playa/lacustrine |
| SP080314-4 | −24.748 | −67.017 | 3650 | 0.16 ± 0.01 | U–Pb zircon | – | 2/47† | – | – | – | – | – | Tuff, playa/lacustrine |
| SP050315-2 | −24.303 | −67.092 | 3674 | 0.16 ± 0.01 | U–Pb zircon | 1.71 | 19/50 | – | – | – | – | – | Tuff, playa/lacustrine |
| SP080314-3 | −24.748 | −67.017 | 3650 | 0.19 ± 0.02 | U–Pb zircon | – | 2/50† | – | – | – | – | – | Tuff, playa/lacustrine |
| SP180315-1 | −24.804 | −66.995 | 3689 | 0.23 ± 0.01 | U–Pb zircon | 2.06 | 32/50 | – | – | – | – | – | Tuff, playa/lacustrine |
| SP160316-4 | −24.308 | −67.086 | 3660 | 0.45 ± 0.03 | U–Th calcite | – | – | – | – | – | – | – | Stromatolite |
| TG120317-3 | −24.616 | −67.366 | 3525 | 0.71 ± 0.05 | U–Pb zircon | – | 1/50† | – | – | – | – | – | Tuff, playa/lacustrine |
| TG130317-1 | −24.641 | −67.370 | 3530 | 0.73 ± 0.01 | U–Pb zircon | 0.14 | 3/50 | – | – | – | – | – | Tuff, playa/lacustrine |
| SP180312-2 | −24.392 | −66.970 | 3719 | 1.54 ± 0.08 | U–Pb zircon | – | 1/31† | – | – | – | – | – | Tuff, alluvial/fluvial |
| SP040315-1 | −24.393 | −66.971 | 3712 | 1.84 ± 0.05 | U–Pb zircon | – | 1/30† | −129.5 | −130.2 | – | −129.8 ± 0.7 | 4.6 ± 0.1 | Tuff, alluvial/fluvial |
| SP090314-2 | −24.386 | −66.973 | 3710 | 3.16 ± 0.05 | U–Pb zircon | 1.97 | 12/49 | −82.4 | −85.5 | – | −83.9 ± 3.1 | 3.8 ± 0.1 | Tuff, alluvial/fluvial |
| SP160316-2 | −24.303 | −67.092 | 3669 | 3.19 ± 0.03 | U–Pb zircon | 2.34 | 20/40 | −117.8 | −119.6 | −118.7 | −118.7 ± 1.0 | 4.7 ± 0.1 | Tuff, alluvial/fluvial |
| SP170316-1 | −24.354 | −67.118 | 3805 | 5.07 ± 0.07 | U–Pb zircon | 1.29 | 6/40 | −119.8 | −119.2 | −120.8 | −120.0 ± 0.9 | 4.7 ± 0.1 | Tuff, playa/lacustrine |
| SP090314-1 | −24.388 | −66.972 | 3720 | 5.24 ± 0.11 | U–Pb zircon | 2.11 | 14/50 | −119.0 | −112.5 | – | −115.7 ± 6.5 | 5.0 ± 0.1 | Tuff, playa/lacustrine |
| SP090314-3 | −24.386 | −66.971 | 3730 | 5.46 ± 0.08 | U–Pb zircon | 2.15 | 10/40 | −83.7 | −83.9 | – | −83.8 ± 0.2 | 6.1 ± 0.0 | Tuff, playa/lacustrine |
| SP170316-2 | −24.355 | −67.116 | 3828 | 6.02 ± 0.03 | U–Pb zircon | 1.25 | 28/30 | −120.0 | −116.2 | −116.6 | −117.6 ± 2.4 | 5.8 ± 0.0 | Tuff, playa/lacustrine |
| SM-A-I | −24.480 | −67.137 | 4000 | 7.77 ± 0.04 | U–Pb zircon | 2.02 | 51/54 | −129.3 | −129.0 | – | −129.1 ± 0.3 | 4.9 ± 0.2 | Tuff, playa/lacustrine |
| SP170316-3 | −24.362 | −67.115 | 3765 | 7.78 ± 0.07 | U–Pb zircon | 2.08 | 18/40 | – | – | – | – | – | Ignimbrite |
| SP050314-2 | −24.353 | −67.128 | 3900 | 8.07 ± 0.08 | U–Pb zircon | 0.49 | 15/50 | – | – | – | – | – | Ignimbrite |
| SP050314-1 | −24.353 | −67.128 | 3900 | 8.31 ± 0.07 | U–Pb zircon | 1.44 | 47/50 | – | – | – | – | – | Ignimbrite |
| SP170316-4 | −24.373 | −67.138 | 3794 | 8.57 ± 0.20 | U–Pb zircon | – | 2/50† | – | – | – | – | – | Tuff, playa/lacustrine |
| RC070314-3 | −24.589 | −67.107 | 3773 | 8.87 ± 0.43 | U–Pb zircon | – | 1/44† | −122.5 | – | – | −122.5 | 6.5 | Tuff, playa/lacustrine |
| PO130317-1 | −24.413 | −66.923 | 4020 | 9.05 ± 0.08 | U–Pb zircon | 1.98 | 12/50 | – | – | – | – | – | Tuff, alluvial/fluvial |
| RC-A-I | −24.581 | −67.094 | 3770 | 12.63 ± 0.25 | U–Pb zircon | – | 2/45† | −102.7 | −108.2 | – | −105.4 ± 5.5 | 8.0 ± 0.5 | Tuff, fluvial |
| QQ130317-1 | −24.414 | −66.934 | 3910 | 13.36 ± 0.06 | U–Pb zircon | 2.06 | 80/140 | – | – | – | – | – | Tuffaceous sandstone |
| RC070314-1 | −24.584 | −67.170 | 3828 | 14.32 ± 0.14 | U–Pb zircon | 1.99 | 28/48 | – | – | – | – | – | Tuff, playa/lacustrine |

*Number of grains selected for age estimation/total number of grains analyzed.
†U–Pb zircon maximum depositional age.
‡For single aliquot samples, uncertainties of 5‰ are assumed.
§Water content based on peak area measurements of NBS-30 replicates and unknowns.

(non-cal. BP). These ages largely confirm the previous regional chronostratigraphy, Fig. 2, e.g., refs. 21, 22, and 65, yet they provide insights into the tectonosedimentary evolution of the central Puna (Fig. 3), which are discussed in the following section. For analytical data, see *SI Appendix*, Tables S4–S12.

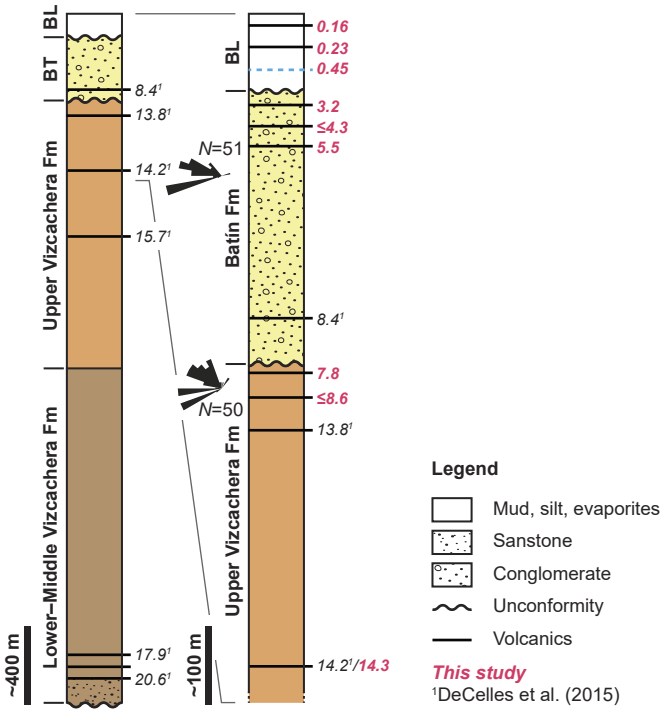


**Fig. 2.** Simplified stratigraphy of the Pocitos area with a representative set of radiometric ages. Rose plots represent paleocurrent directions from imbricated clast measurements. BT, Batín Formation; BL, Blanca Lila Formation. Note: The *Right* column shows an enlarged excerpt of the *Left* column.

**Hydrogen Stable Isotopes.** Our δDg values of volcanic ash deposits in the Siete Curvas/Pocitos area range from about –130 to –84‰ (Table 1). Together with previously published δDg data from the Arizaro, Siete Curvas, and Pastos Grandes basins, *SI Appendix*, Table S13 and Fig. S3, (33, 41, 70), the δDg data can be roughly grouped into two main sets: 1) relatively high δDg values between –110‰ and –90‰ prior to 10 Ma; and 2) relatively low δDg values, clustering between –130‰ and –110‰ after about 9 Ma (*SI Appendix*, Fig. S3*A*).

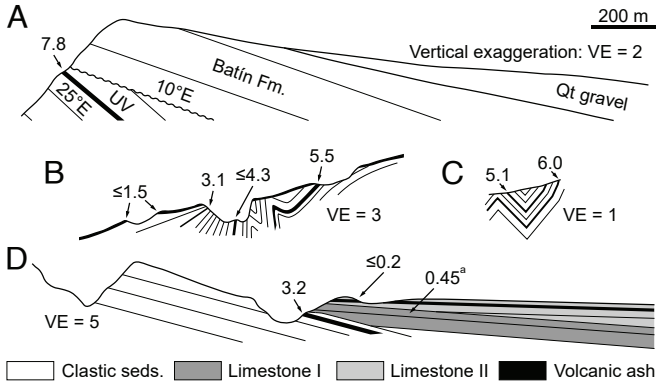


**Fig. 3.** Simplified W–E cross-sections of key localities documenting Mio–Pleistocene deformation in the Pocitos Basin. Numbers refer to obtained U–Pb zircon and U–Th calcite[a] ages in Ma. For profile locations see Fig. 1*C*.

## Discussion

**Miocene to Pleistocene Deformation.** Evidence for middle to late Miocene deformation of the Pozuelos Range along the eastern margin of the Pocitos Basin is provided by tilted strata in the Quebrada Quirón (black star in Fig. 1*C*). Here, tightly folded and incised Ordovician basement rocks are unconformably overlain by tilted (070/38°), ca. 35-m-thick sandstones and conglomerates mainly composed of proximal basement-rock clasts (*SI Appendix*, Figs. S1*A* and S2). Based on U–Pb zircon geochronology of a tuffaceous sandstone intercalated within this sequence, deposition occurred at 13.4 ± 0.1 Ma (QQ130317-1, Table 1), postdating the onset of late Cenozoic range uplift and exhumation/incision of the Pozuelos Range. These conglomerates are in turn unconformably overlain by less tilted gravels (070/10°) interbedded with a 9.1 ± 0.1-Ma tuff (PO130317-1), documenting continued deformation along the range-bounding Pozuelos Fault until after 9 Ma.

Moreover, west of the Quevar volcanic center, at the northern continuation of the Pozuelos Fault (B–B' in Fig. 1*C* and Fig. 3*B*), ash-bearing folded sedimentary and volcaniclastic deposits, previously mapped as the Geste Formation (28), yielded ages from 5.5 ± 0.1 Ma (SP090314-3) to 1.5 ± 0.1 Ma (SP180312-2). Upward-decreasing stratal dips indicate syn-depositional growth of an anticline that continues northward and deforms alluvial-fan deposits as young as 0.15 ± 0.03 Ma (SP160316-3). Hence, our observations at the eastern margin of the Pocitos Basin suggest that deformation has been ongoing for at least 13 My and has remained active until the present day.

Along the Colorados Range, at the border between the Pocitos and Siete Curvas areas (A–A' in Fig. 1*C*, Fig. 3*A*, and *SI Appendix*, Fig. S1*B*), a tuff from a 25°E-dipping section of the Upper Vizcachera Formation was dated to 7.8 ± 0.1 Ma (SM-A-1). These beds are unconformably overlain by 10°E-dipping conglomerates of the Batín Formation. A similar observation is made about 10 km to the north, where 75°E-tilted Upper Vizcachera strata, dated at 8.6 ± 0.2 Ma (SP170316-4), are unconformably overlain by the Batín Formation. Here, upward decreasing dips from 60 to 20°E clearly indicate structural growth during the deposition of the Batín Formation (ca. 8–3 Ma). This regional angular unconformity is important because it postdates the onset of significant crustal shortening in the Arizaro and Pocitos areas, which must have occurred sometime after ca. 8 Ma, as our age estimates of tuffs in the Upper Vizcachera Formation indicate.

The northern Salar de Pocitos is bordered to the west by an unnamed north-south trending structural ridge (up to 500 m above the basin floor, labeled "X-Ridge" in Fig. 1*C*) whose folded and uplifted volcanic rocks of the Miocene Tajamar Formation (28) dip eastward (in places 40°E) below the playa surface. U–Pb geochronology of ignimbrites intercalated in these deposits at the southern tip of this range confirms their late Miocene origin (SP050314-2: 8.1 ± 0.1 Ma, SP170316-3: 7.8 ± 0.1 Ma). These volcanic rocks are partially overlain by strongly folded Miocene–Pliocene (SP170316-2: 6.0 ± 0.1 Ma, SP170316-1: 5.1 ± 0.1 Ma) fine-grained gypsiferous redbeds, indicating considerable shortening (C–C' in Fig. 1*C* and Fig. 3*C*). Outcrops to the east of the "X-Ridge," along the northwestern margin of the Salar de Pocitos, show E-dipping playa sediments (i.e., interbedded sandstones and stromatolitic limestone beds) of the Blanca Lila Formation with intercalated ashes and reworked ash overlying volcanic rocks (D–D' in Fig. 1*C*, Fig. 3*D*, and *SI Appendix*, Fig. S1*D*). The uppermost horizons of these volcanic rocks dip 10–12°E and contain a 3.2 ± 0.1 Ma volcanic ash (SP160316-2). U–Th calcite geochronology of an overlying stromatolitic limestone provided a mean age of 0.45 ± 0.03 Ma. Finally, U–Pb zircon geochronology of an intercalated ash in the uppermost, 5°E-dipping section yielded an age of 0.16 ± 0.01 Ma (SP050315-2). Hence, upsection-decreasing dips clearly document Plio-Pleistocene structural growth in this sector of the basin.

Field observations reveal multiple step-like terrace levels in the Pocitos Basin at successively lower elevations relative to the basin floor that are associated with relative lake-level changes during the Quaternary (71) and can be tentatively correlated with glacial advances and thus greater water availability constrained by surface-exposure dating on moraine deposits on the nearby Quevar volcano (72). Along the western margin of Salar de Pocitos, these paleoshorelines are more frequent, ca. 2.5 to 5 m higher, and better preserved than along the eastern margin that is more characterized by gentle piedmonts of the southwestern Pozuelos Range associated with alluvial-fan surfaces graded to the playa. The asymmetry in the distribution of the terrace treads suggests continued growth of the anticline, whose eastern flank constitutes the Colorados Range.

Radiometric ages of elevated and exposed strata of the Blanca Lila Formation along the western margin of the Salar de Pocitos range from 0.23 to 0.04 Ma (Fig. 1*C*) and support the interpretation of Pleistocene deformation in the study area. Similarly, symmetric open folds (TG130317-1: 0.73 ± 0.01 Ma) and potentially raised shorelines (TG120317-3: 0.71 ± 0.05 Ma) in tuffaceous deposits of the Blanca Lila Formation in the Arizaro Basin along the western foothills of the Macón Range record late Quaternary deformation.

Based on these observations, we suggest that the Arizaro-Pocitos area between ca. 24 and 25°S has been governed by shortening during the Quaternary. This is similar to observations in the adjacent Pastos Grandes Basin to the east, (e.g., ref. 41), making this Andean section unique compared to the northern and southern sectors of the Puna Plateau, which show evidence for tectonically neutral and/or extensional settings, respectively, e.g., refs. 66, 73, and 74.

**Paleoaltimetry.** In this study, we integrate all available volcanic glass stable isotope data ($\delta$Dg) from the central Puna between ca. 24°S and 25°S (33, 41, 70, this study) and (re)examine their implications within the context of surface uplift compared to the low-elevation foreland, [Fig. 4, (40, 41)]. This "$\delta$–$\delta$ approach" relates ancient $\delta$Dg values from a high-elevation proxy record of unknown elevation with those from an upwind site at low elevation aiming to minimize confounding effects of climate change on the isotopic composition of the moisture source. Consequently, the difference in $\delta$Dg ($\Delta\delta$Dg) should largely reflect the elevation difference between the two sites, (e.g., ref. 37). As a low elevation baseline, we use $\delta$Dg data from the eastern flank of the Andes, published in Pingel et al. (40, 41), which show no significant shifts in $\delta$Dg, indicating a consistent moisture source and potentially constant elevation since at least 14 Ma (Fig. 4). For completeness, we incorporate published $\delta$Dg data and paleoaltimetry interpretations from the intervening Quebrada del Toro Basin in the Eastern Cordillera [Fig. 4, (41)].

Previous paleoaltimetry studies suggest close to present-day elevations of the central and southern Puna (ca. 3.5 to 4 km) since the late Eocene (33, 70). Specifically, Quade et al. (33) report relatively constant $\delta$Dg values (mean $\delta$Dg: –90 ± 6‰) from the Arizaro Basin and Siete Curvas between 34.8 and 0.4 Ma, leading the authors to deduce no significant change

in elevation. However, Mio–Pleistocene proxy records from the Andean Plateau are generally characterized by a much broader $\delta$Dg range (–130‰ to –30‰), strongly suggesting evaporative enrichment (higher $\delta$Dg) in the high and dry plateau region for many of the samples, e.g., refs. 38 and 41, this study. This effect has been demonstrated for modern surface waters of the Altiplano and is assumed to have significant implications for paleoaltimetry studies conducted in arid environments (76, 77). By focusing on the most negative $\delta$Dg values, the effects of evaporation on the hydrogen isotope record can thus be minimized, increasing the likelihood of obtaining unbiased signals of ancient precipitation, which are essential for accurate paleoaltimetry estimates (38, 41, 76, 77).

Using this approach, we show that the central Puna has not been at high elevation since the Eocene (Fig. 4*B*). Our $\delta$Dg data compilation from the central Puna exhibits significant variability since 10 Ma (*SI Appendix*, Fig. S3), likely indicating heavy isotope enrichment ($\delta$Dg > –120‰), consistent with the late Miocene emergence of orographic aridity in the central Puna (22, 78). After removing samples with a potentially heavy isotope-enriched signature, three notable sample populations become apparent: 1) 35–13 Ma, mean $\delta$Dg –93 ± 3‰ (SD), 2) 13–10 Ma, mean $\delta$Dg –106 ± 1‰ (SD); and 3) <10 Ma, mean $\delta$Dg –126 ± 3‰ (SD) (Fig. 4). For more information on evaporative enrichment, see *SI Appendix*.

Our $\delta$Dg data from the Pocitos Basin and Siete Curvas complement previous studies at this latitude by reproducing systematic temporal trends in $\delta$Dg that have previously been interpreted to signal km-scale surface uplift of the Pastos Grandes Basin between ca. 10–8 Ma (41). Moreover, our $\delta$Dg data hints toward an earlier onset of surface uplift at ca. 13 Ma, suggesting in total a $\delta$Dg shift of –34 ± 4‰ since the middle Miocene. When applying the modern regional isotopic lapse rate of –15.8 ± 7.9‰ (40, 75), this shift represents an average surface uplift of ca. 2.1 ± 1.1 km between 13 and 10 Ma (Fig. 4*A*). This suggests that during the Eocene, the central Puna region could not have been located near its current elevation of ca. 4 km, but rather at half of this altitude (1.9 ± 0.6 km asl). This inference is supported by paleoenvironmental conditions during deposition of the regionally widespread Geste Formation, whose lateritic paleosols and marsupial, notoungulate, and various reptile fossils indicate a rather warm, humid climate at relatively low elevation (60, 79–81), potentially in a broken-foreland setting (7).

In addition, two middle Miocene (ca. 18 Ma) samples from the eastern flanks of the Quebrada del Agua Range (70) show a significant negative offset compared to the age-equivalent Puna basin records (Fig. 4*A*). This difference suggests that these samples may have been hydrated by ambient water associated with higher topography of the Western Cordillera. The mean $\delta$Dg is –111 ± 7‰ (SD) indicating an elevation difference between the foreland and this region of 2.0 ± 1.1 km at an absolute elevation of 3.1 ± 1.1 km asl. This is about 1.5 km lower than the present-day average elevation of the Western Cordillera (ca. 4.5 km asl), suggesting a not further specified continuation of surface uplift after 18 Ma. A similar setting is documented in Jimenez-Rodriguez et al. (82), who see evidence for near-modern elevations in the Western Cordillera of northern Chile since ca. 23 Ma.

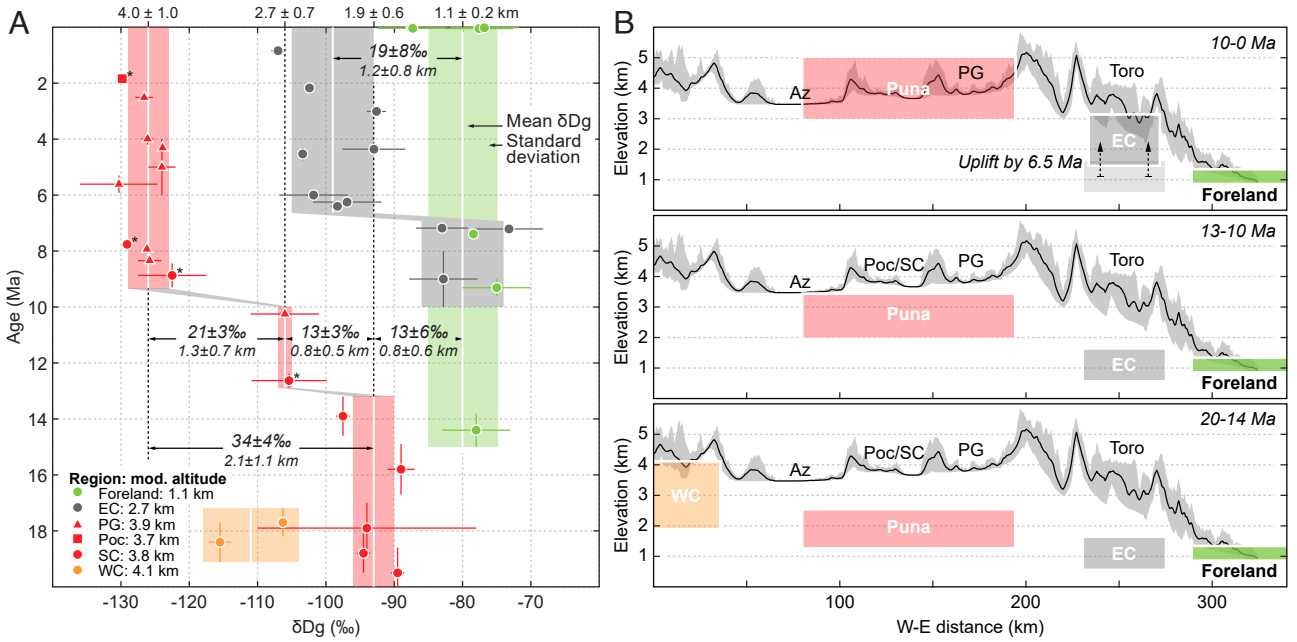


**Fig. 4.** Hydrogen stable isotope data and paleoaltimetry estimates for the southern Central Andes (24–25°S). (*A*) $\delta$Dg vs. depositional age (±2$\sigma$ error bars) from the low-elevation foreland [green, (41)], Eastern Cordillera [gray, (41)], Puna Plateau [red, (33, 41) this study], and Western Cordillera [WC, orange, (70)]. Asterisks indicate data from this study. Data excluded from paleoaltimetry calculations are presented in *SI Appendix*, Table S13 and Fig. S3. Note the stepwise decrease in $\delta$Dg in the Puna records, which we interpret to reflect surface uplift. Assuming an isotopic lapse rate of –15.8 ± 7.9‰/km (75), the isotopic difference of 34 ± 4‰ between the pre-13 Ma and post-10 Ma Puna implies an elevation gain of about 2.1 ± 1.1 km (from ca. 1.9 to 4.0 km asl). (*B*) Schematic illustration of the paleotopographic evolution across the southern Central Andes (Az–Arizaro, Poc/SC–Pocitos/Siete Curvas, and PG–Pastos Grandes). Colored bars show representation of paleotopography estimates for each time period calculated from the isotopic difference ($\Delta\delta$Dg) between the foreland and the region of interest (*SI Appendix*, Table S14). The black curve and gray envelope show modern topography (min, mean, max) across the swath area shown in Fig. 1*B*. 20–14 Ma: While the present-day foreland and the Eastern Cordillera are at a similar elevation of about 1.1 ± 0.4 km (41) and 1.1 ± 0.2 km asl, respectively, the Puna Plateau is at about 1.9 ± 0.6 km asl. Limited data from the Western Cordillera indicate paleoelevations of 3.1 ± 1.1 km asl; 13–10 Ma: The Puna Plateau experiences surface uplift on the order 0.8 ± 0.5 km from ca. 1.9 to 2.7 km asl; 10–0 Ma: Between 9 and 8 Ma, the central Puna Plateau attained modern elevations of 4.0 ± 1.0 km asl, and although the Eastern Cordillera was deformed as early as the middle Miocene ca. 13 Ma, e.g., ref. 25, signs of significant surface uplift to modern elevations (2.3 ± 0.7 km asl) are not evident until about 6.5 Ma (41).

**Tectonic Evolution.** Thermochronologic and tectonosedimentary studies between about 24 and 25°S have documented a more than 250-km-wide zone affected by Eocene deformation and spatially disparate basement uplifts from the Western Cordillera to the Eastern Cordillera (e.g., refs. 7 and 24 and *SI Appendix*, Fig. S4 and Table S2). As discussed in the following section (Geodynamic implications), the topographic relief of these ranges must have been relatively low, considering abundant evidence for Eocene reburial and primarily low-angle growth structures within the regional Eocene foreland strata.

For example, low-temperature thermochronology performed on Ordovician granites—partly overlain by strata of the Eocene Geste Formation—along the western margin of the Arizaro Basin [herein referred to as the Quebrada del Agua Range, (21, 83)] and the Macón granite (84) suggests Eocene exhumation. Similarly, regional onlap relationships between the Ordovician basement of the Copalayo Range and the Geste Formation, as well as potential intraformational growth strata, suggest basement exposure and range uplift during the Eocene along the western margin of the present-day Pastos Grandes Basin, e.g., refs. 21, 51, 67, and 85. Farther east, in the La Poma and Quebrada del Toro basins at the eastern Puna margin, syn-sedimentary deformation is observed in the middle to late Eocene Quebrada de los Colorados Formation (86, 87).

The widespread occurrence of the Oligo–Miocene Vizcachera Formation across the Arizaro and Pocitos basins and partly contemporaneous units, i.e., the Quebrada del Agua Formation near the western margin of the Arizaro Basin (88, 89) and the Pozuelos Formation in the Pastos Grandes Basin (this study), suggests burial of previously exposed basement rocks since ca. 20 Ma. This is for example documented by unconformable onlap of the Vizcachera Formation over basement rocks of the Macón and Pozuelos ranges [Fig. 1*C*, (21, 29)].

Late Cenozoic deformation along the Quebrada del Agua Range is constrained by growth strata in ca. 23–15 Ma volcaniclastic deposits of the Quebrada del Agua Formation in the hanging wall of an east-verging reverse fault (88, 89). Final exhumation of the Copalayo Range is approximated by detrital apatite (U–Th)/He thermochronology to ca. 15–10 Ma (51), consistent with potential growth strata in ca. 17–13 Ma volcaniclastic and conglomeratic beds of the Catal Formation along the eastern flanks of the Ratones Range (66).

For the adjacent Pozuelos Range, we infer a similar timing of rock uplift and exhumation, constrained to 16–13 Ma, based on: a) the proximity to the Copalayo Range; b) deformed Middle Vizcachera Formation [17.5–16 Ma, (21)] overlying the Ordovician Copalayo Formation at the southern tip of the Pozuelos Range, (e.g., ref. 29), indicating that late Cenozoic uplift and deformation occurred after ca. 16 Ma; and c) deformed 13.4 Ma fluvial sediments deposited over a previously exposed paleorelief sculpted into the Ordovician basement (Quebrada Quirón; see *SI Appendix*, Fig. S2), suggesting uplift commenced prior to about 13 Ma.

Final exhumation of the Macón Range to the west commenced about 10 ± 5 Ma (21, 51). Significant deformation in the intervening Pocitos Basin must have occurred at about 8 Ma, as indicated by the regional unconformity separating the strongly folded Upper Vizcachera Formation from the less tilted Batín Formation, which suggests a causal link between range uplift and basin-internal shortening.

Interestingly, the middle to late Miocene deformation obse -rved in the central Puna largely coincides with the onset of late Cenozoic deformation in the Eastern Cordillera, resulting in an at least 200-km-wide zone (from the Macón to the Mojotoro range) of active deformation since ca. 15–10 Ma (Fig. 1*B* and *SI Appendix*, Fig. S4).

Above, we documented various sites across the Pocitos Basin recording Miocene and younger deformation associated with shortening (see Miocene to Pleistocene deformation). Similar observations can be made in the adjacent Pastos Grandes Basin, where late Miocene sediments of the Sijes Formation (8–7 Ma) are unconformably overlain by the conglomeratic Singuel Formation (6–2.5 Ma) (41). Both units are strongly deformed and overlain by the Pleistocene Blanca Lila Formation (41, 78, 90), which also records minor faulting and folding (66). Miocene to Quaternary shortening is also documented along the western and eastern margins of the Arizaro Basin [(21, 89), this study].

**Geodynamic Implications.** Previous studies proposed a geodynamic model for the tectonosedimentary evolution of the Miocene Arizaro-Pocitos Basin in which thickened lower crust underwent progressive eclogitization, drip formation, and foundering, e.g., refs. 19 and 21. As a result, the surface above the lithospheric drip has subsided since ca. 19 Ma, forming accommodation space for thick sediment deposition (i.e., the ca. 24–8 Ma Vizcachera Formation). Numerical and analog models demonstrate that sustained subsidence in this setting could lead to significant upper crustal shortening, followed by rebound and topographic inversion upon drip release—as proposed for the Miocene Arizaro-Pocitos Basin, around ca. 7 Ma (19–21, 91). A key assumption for this model is that the crust of the Puna Plateau was already thickened prior to 20 Ma, e.g., 19 and 20, derived from two lines of reasoning: 1) near-modern elevations of the Puna since the Eocene (33, 70); and 2) Eocene shortening and crustal thickening in the present-day Puna Plateau, (e.g., ref. 85).

Near-modern elevations since the Eocene are neither supported by the stable-isotope data nor by the paleoenvironmental observations presented or cited here. Instead, the area of the present-day central Puna Plateau appears to have been at relatively low elevation during the Eocene compared to today, and it was not until between 13 and 10 Ma that significant surface uplift occurred. This observation requires a geodynamic framework that allows for surface uplift, which the current drip models of Wang et al. (19, 20) do not support.

Here, we propose an alternative evolutionary model for the central Puna region at 24–25°S in which crustal shortening and thickening since 20 Ma led to the formation of a dense crustal root, followed by lower lithospheric delamination in the middle to late Miocene, and subsequent asthenospheric upwelling that caused rapid, km-scale surface uplift between 13 and 10 Ma, as seen in our $\delta$Dg record. This inference is broadly consistent with a previously proposed model for the evolution of the Quebrada del Toro Basin in the Eastern Cordillera at 24.5°S in which crustal shortening caused thickening of the lithosphere by ca. 13–11 Ma followed by delamination and associated backarc volcanism at ca. 11–6 Ma (18). Similarly, Acocella et al. (17) suggested piecemeal lithospheric delamination including at least two possible episodes of delamination-derived magmatism along the Calama–Olacapato–El Toro magmatic belt at 12–11 Ma and after 1.5 Ma.

While there is unambiguous evidence for Eocene crustal shortening in the Puna region, e.g., 7 and 24, the impact of this shortening phase on crustal thickness evolution and the construction of plateau topography is not well understood. Many mountain ranges whose bounding faults were active during the Eocene show evidence of syn- and/or postdeformational deposition and burial by regionally distributed middle to late Eocene redbeds and conglomerates of the Geste Formation in the southern Puna and the Quebrada de los Colorados Formation

in the Eastern Cordillera; this is also suggested by the deposits comprising the Casa Grande Formation in the northern Puna and the adjacent Eastern Cordillera. These observations, combined with the fact that most documented angular unconformities associated with Eocene strata exhibit relatively low angles, (e.g., refs. 7, 26, 63, 86, and 92), indicate that the topographic relief of these ranges may have been neither very pronounced nor laterally extensive during that time. Further potential evidence for low topography comes from thermal models and structural reconstructions, which imply that some of these mountain ranges experienced multiple episodes of exhumation with intermediate heating during Eocene sedimentary burial (51, 93–95).

These considerations suggest that lithospheric foundering via the proposed RT-drip formation at about 20 Ma, which is thought to have initiated sedimentation of the late Oligocene to Miocene Vizcachera Formation (21), may not be a prerequisite for the tectonosedimentary patterns observed in the Arizaro-Pocitos area. Moreover, formation of the RT-drip coincides with extensive contemporaneous contractional deformation and basement uplift in the present-day Puna region since ca. 20 Ma (Fig. 1*B* and *SI Appendix*, Fig. S4). For example, deformation along the present-day Puna margin (Cumbres de Luracatao) resulted in structural separation of the Puna from the foreland after ca. 20 Ma (23, 93, 96). Furthermore, deformation affected: a) the Tanque and Lina ranges at ca. 20 Ma to the north (24); b) the Sierra Laguna Blanca in the southern Puna [≤20 Ma, (97)]; c) the Pocitos and Copalayo/Ratones ranges east of the Pocitos Basin at ca. 15–10 Ma [this study, (51)]; and d) the Quebrada del Agua Range (western Arizaro Basin margin) between ca. 23–15 Ma (88, 89). These uplifts may have led to structural separation and sedimentological isolation of the formerly contiguous sectors of the Puna region, resulting in the formation of accommodation space and deposition of the Vizcachera Formation since ca. 20 Ma. Moreover, our observations indicate continuous contraction since about 10 Ma in the Pocitos area, which is inconsistent with the RT-drip model by Wang et al. (19) that predicts root detachment at about 7 Ma associated with neutral to extensional tectonism at the surface.

On a larger regional scale, our preferred tectonic history model for the central Puna aligns well with both the paleoelevation history of the southern Altiplano at 19 to 22°S discussed in Garzione et al. (98) and the geologically constrained surface uplift history of the western Andean flank adjacent to the northern Puna at 22 to 25°S (99).

## Conclusions

Hydrogen stable-isotope data that we obtained from hydrated volcanic glass in the Pocitos Basin on the Puna Plateau of northwestern Argentina suggest km-scale surface uplift toward present-day elevations since the middle Miocene (ca. 13–10 Ma). This clearly indicates that the central Puna and possibly the southern Puna have not been at high elevation since the Eocene, as previously proposed. This information is crucial for understanding the paleoclimatic conditions associated with orographic barrier formation, as well as for future research exploring biotic pathways, speciation patterns, and the geodynamic framework of the southern Central Andes.

In addition, evidence of ongoing contractional deformation in the Pocitos area supports the notion of continuous active crustal shortening in the central Puna from the middle Miocene until today, while adjacent sectors of the Puna Plateau are characterized by neutral to extensional tectonic settings, e.g., refs. 24 and 74.

In light of our data and previously published information, we suggest that shortening since the early Miocene (ca. 20 Ma) resulted in crustal thickening and the formation of a dense crustal root. This process may have ultimately triggered lithospheric delamination between ca. 15 and 10 Ma, associated with backarc volcanism and upwelling of asthenospheric mantle to cause rapid surface uplift of the central Puna Plateau.

## Materials and Methods

We collected 26 tuffs and tuffaceous layers intercalated with the Mio–Pleistocene sedimentary sequence for U–Pb zircon geochronology. Following standard magnetic and heavy-liquid mineral separation, zircons were handpicked, mounted in epoxy, and polished for U, Th, and Pb isotope analysis using a Laser Ablation Multi-Collector Inductively Coupled Plasma Mass Spectrometer (LA-MC-ICPMS), during 7 analytical sessions (*SI Appendix*, Table S1), at the University of California, Santa Barbara, CA, USA. Due to potentially significant pre-eruptive residence times and/or posteruptive reworking, most analyzed samples show a complex pattern of U–Pb zircon age distributions. Therefore, we systematically excluded the oldest ages from our calculations of an average zircon crystallization age until near-unity values for the mean square of weighted deviates (MSWD $< 2$) were achieved. In cases where no coherent young population was found, we selected the youngest $^{206}Pb/^{238}U$ zircon ages to infer a maximum depositional age (*SI Appendix*, Tables S4–S10).

In addition, we collected a limestone sample from a tilted stromatolitic layer of the Blanca Lila Formation exposed in the northern Salar de Pocitos for U–Th calcite dating at the Massachusetts Institute of Technology, Cambridge, MA, USA (*SI Appendix*, Table S11), and a calcrete layer capping minor terraces at the western shore of the Salar de Pocitos for AMS $^{14}C$ dating (*SI Appendix*, Table S12).

Where possible, glass shards were extracted from volcanic ash samples to perform $\delta Dg$ analyses ($N = 10$). For this purpose, volcanic ash and ignimbrite samples were crushed, sieved, and cleaned with 10% hydrochloric acid for 15 min and 5% hydrofluoric acid for 30 s in an ultrasonic bath. Following standard magnetic and density techniques, glass shards (250 to 500 μm) were handpicked using a cross-polarizing microscope. About 1.5 mg of glass per aliquot was packed in silver cups, loaded, and released to a helium-purged Thermo-Finnigan TC/EA (high-temperature conversion/elemental analyzer) equipped with a Costech zero-blank autosampler. The extracted sample gas was admitted into a Thermo-Finnigan ConFlo III connected in continuous-flow mode to a Thermo-Finnigan MAT 253 stable-isotope mass-spectrometer. All isotope measurements were performed at the Joint Goethe University-Senckenberg BiK-F Stable Isotope Facility, Frankfurt, Germany. All isotopic ratios are reported relative to V-SMOW (Table 1). Information on reference materials and water-content calculation can be found in *SI Appendix*.

**Data, Materials, and Software Availability.** Locations of all geochronological and stable isotope samples used in this study. Data have been deposited in Figshare (https://www.doi.org/10.6084/m9.figshare.24076044) (100). All other data are included in the manuscript and/or *SI Appendix*.

**ACKNOWLEDGMENTS.** This research was funded by Deutsche Forschungsgemeinschaft (DFG) grants STR373/21-1 and STR373/16-1 to Strecker and MU2845/4-1 to Mulch. Additional support came from DFG grant STR373/34-1 and the Brandenburg Ministry of Sciences, Research and Cultural Affairs, Germany, within the framework of the international research training group IGK2018 SuRfAce processes, TEctonics and Georesources: The Andean foreland basin of Argentina (StRATEGy). We thank C.Y. Chen (MIT) for U–Th calcite dating, L. Luna, P. Lanouette, B. Purinton, A. Rosner, and M. Lang (U Potsdam) for field assistance, and Y. Rojo for logistical support. We wish to thank the two anonymous reviewers for their detailed and constructive reviews.

Author affiliations: [a]Universität Potsdam, Institut für Geowissenschaften, Potsdam 14476, Germany; [b]Facultad de Ciencias Naturales, Universidad Nacional de Salta, Salta 4400, Argentina; [c]Department of Earth Science, University of California, Santa Barbara, CA 93106; [d]Senckenberg Biodiversität und Klima Forschungszentrum, Frankfurt/Main 60325, Germany; [e]Goethe Universität Frankfurt, Institut für Geowissenschaften, Frankfurt/Main 60438, Germany; and [f]Institute of Geological Sciences, Freie Universität Berlin, Berlin 12249, Germany

1. R. W. Allmendinger, T. E. Jordan, S. M. Kay, B. L. Isacks, The evolution of the Altiplano-Puna Plateau of the Central Andes. *Annu. Rev. Earth Planet. Sci.* **25**, 139–174 (1997).
2. T. E. Jordan *et al*., Andean tectonics related to geometry of subducted Nazca plate. *GSA Bull.* **94**, 341–361 (1983).
3. R. Kay, S. M. Kay, Delamination and delamination magmatism. *Tectonophysics* **219**, 177–189 (1993).
4. S. M. Kay, B. Coira, J. Viramonte, Young mafic back arc volcanic rocks as indicators of continental lithospheric delamination beneath the Argentine Puna Plateau, Central Andes. *J. Geophys. Res.: Solid Earth* **99**, 24323–24339 (1994).
5. C. N. Garzione, P. Molnar, J. C. Libarkin, B. J. MacFadden, Rapid late Miocene rise of the Bolivian Altiplano: Evidence for removal of mantle lithosphere. *Earth Planet. Sci. Lett.* **241**, 543–556 (2006).
6. P. G. DeCelles, B. Carrapa, B. K. Horton, G. E. Gehrels, Cenozoic foreland basin system in the Central Andes of northwestern Argentina: Implications for Andean geodynamics and modes of deformation. *Tectonics* **30**, 1–30 (2011).
7. C. Montero-López *et al*., Development of an incipient Paleogene topography between the present-day Eastern Andean Plateau (Puna) and the Eastern Cordillera, Southern Central Andes. *NW Argentina. Basin Res.* **33**, 1194–1217 (2021).
8. B. K. Horton, Tectonic regimes of the Central and Southern Andes: Responses to variations in plate coupling during subduction. *Tectonics* **37**, 402–429 (2018).
9. B. Schurr, G. Asch, A. Rietbrock, R. Trumbull, C. Haberland, Complex patterns of fluid and melt transport in the Central Andean subduction zone revealed by attenuation tomography. *Earth Planet. Sci. Lett.* **215**, 105–119 (2003).
10. F. J. Calixto *et al*., Velocity structure beneath the southern Puna Plateau: Evidence for delamination. *Geochem. Geophys. Geosyst.* **14**, 4292–4305 (2013).
11. B. Heit *et al*., Structure of the crust and the lithosphere beneath the southern Puna Plateau from teleseismic receiver functions. *Earth Planet. Sci. Lett.* **385**, 1–11 (2014).
12. A. Scire, C. B. Biryol, G. Zandt, S. Beck, "Imaging the Nazca slab and surrounding mantle to 700 km depth beneath the central Andes (18°S to 28°S)" in *Geodynamics of a Cordilleran Orogenic System: The Central Andes of Argentina and Northern Chile*, P. DeCelles, M. N. Ducea, B. Carrapa, P. Kapp, Eds. (Geological Society of America, 2015).
13. Y. Gao *et al*., Full waveform inversion beneath the Central Andes: Insight into the dehydration of the Nazca slab and delamination of the back-arc lithosphere. *J. Geophys. Res.: Solid Earth* **126**, 1–32 (2021).
14. S. L. Beck, G. Zandt, K. M. Ward, A. Scire, "Multiple styles and scales of lithospheric foundering beneath the Puna Plateau, Central Andes in Geodynamics of a Cordilleran Orogenic System" in *The Central Andes of Argentina and Northern Chile*, P. DeCelles, M. N. Ducea, B. Carrapa, P. Kapp, Eds. (Geological Society of America, 2015), pp. 43–60.
15. J. Chen *et al*., Lithospheric delamination beneath the southern Puna Plateau resolved by local earthquake tomography. *J. Geophys. Res.: Solid Earth* **125**, e2019JB019040 (2020).
16. A. Tassara, H. J. Götze, S. Schmidt, R. Hackney, Three-dimensional density model of the Nazca plate and the Andean continental margin. *J. Geophys. Res.: Solid Earth* **111**, B09404 (2006).
17. V. Acocella *et al*., Tectonomagmatic characteristics of the back-arc portion of the Calama-Olacapato-El Toro Fault Zone. *Central Andes. Tectonics* **30**, TC3005 (2011).
18. R. Mazzuoli *et al*., Miocene magmatism and tectonics of the easternmost sector of the Calama-Olacapato-El Toro fault system in Central Andes at 24°S: Insights into the evolution of the Eastern Cordillera. *GSA Bull.* **120**, 1493–1517 (2008).
19. H. Wang, C. A. Currie, P. G. DeCelles, "Hinterland basin formation and gravitational instabilities in the Central Andes: Constraints from gravity data and geodynamic models in Geodynamics of a Cordilleran Orogenic System" in *The Central Andes of Argentina and Northern Chile*, P. DeCelles, M. N. Ducea, B. Carrapa, P. Kapp, Eds. (Geological Society of America, 2015).
20. H. Wang, C. A. Currie, P. G. DeCelles, Coupling between lithosphere removal and mantle flow in the Central Andes. *Geophys. Res. Lett.* **48**, e2021GL095075 (2021).
21. P. DeCelles *et al*., "The Miocene Arizaro Basin, central Andean hinterland: Response to partial lithosphere removal?" in *Geodynamics of a Cordilleran Orogenic System: The Central Andes of Argentina and Northern Chile*, P. DeCelles, M. N. Ducea, B. Carrapa, P. Kapp, Eds. (Geological Society of America, 2015).
22. R. N. Alonso, T. E. Jordan, K. T. Tabbutt, D. S. Vandervoort, Giant evaporite belts of the Neogene Central Andes. *Geology* **19**, 401–404 (1991).
23. I. Coutand *et al*., Propagation of orographic barriers along an active range front: Insights from sandstone petrography and detrital apatite fission-track thermochronology in the intramontane Angastaco basin, NW Argentina. *Basin Res.* **18**, 1–26 (2006).
24. H. Pingel *et al*., Cenozoic exhumation and deformation of the intermontane Pastos Chicos Basin in the southern Central Andes: Implications for the tectonic evolution of the Andean Plateau (Puna) and the Eastern Cordillera between 23 and 24°S, NW Argentina. *Tectonics* **42**, e2022TC007487 (2023).
25. D. M. Pearson *et al*., Influence of pre-Andean crustal structure on Cenozoic thrust belt kinematics and shortening magnitude: Northwestern Argentina. *Geosphere* **9**, 1766–1782 (2013).
26. P. Payrola, J. Powell, C. del Papa, F. Hongn, Middle Eocene deformation-sedimentation in the Luracatao Valley: Tracking the beginning of the foreland basin of northwestern Argentina. *J. South Am. Earth Sci.* **28**, 142–154 (2009).
27. R. N. Alonso, Estratigrafía del Cenozoico de la cuenca de Pastos Grandes (Puna Salteña) con énfasis en la Formación Sijes y sus boratos. *Revist. Asoc. Geol. Argent.* **47**, 189–199 (1992).
28. G. Blasco, E. O. Zappettini, F. D. Hongn, Hoja Geológica 2566-I, San Antonio de los Cobres, provincias de Jujuy y de Salta. *Bolet. Inst. Geol. Recurs. Miner. Ser. Geol. Minero Argent.* **217**, 1–126 (1996).
29. V. R. Martínez, R. N. Alonso, C. I. Galli, Historia evolutiva paleoambiental del depocentro del salar de Pozuelos (Puna Austral). *Serie Correl. Geol.* **34**, 42–55 (2018).
30. T. E. Jordan, C. Mpodozis, Estratigrafía y evolución tectónica de la cuenca Paleógena de Arizaro-Pocitos, Puna Occidental (24°-25°S). *Actas del XI Congreso Geol. Chileno* **2**, 57–60 (2006).
31. A. Mulch, C. P. Chamberlain, The rise and growth of Tibet. *Nature* **439**, 670–671 (2006).
32. A. Mulch, A. M. Sarna-Wojcicki, M. Perkins, C. Chamberlain, A Miocene to Pleistocene climate and elevation record of the Sierra Nevada (California). *Proc. Natl. Acad. Sci. U.S.A.* **105**, 6819–6824 (2008).
33. J. Quade *et al*., "The growth of the central Andes, 22°S-26°S" in *Geodynamics of a Cordilleran Orogenic System: The Central Andes of Argentina and Northern Chile*, P. DeCelles, M. N. Ducea, B. Carrapa, P. Kapp, Eds. (Geological Society of America, 2015).
34. E. J. Cassel, S. A. Graham, C. P. Chamberlain, Cenozoic tectonic and topographic evolution of the northern Sierra Nevada, California, through stable isotope paleoaltimetry in volcanic glass. *Geology* **37**, 547–550 (2009).
35. E. J. Cassel, D. O. Breecker, C. D. Henry, T. E. Larson, D. F. Stockli, Profile of a paleo-orogen: High topography across the present-day Basin and Range from 40 to 23 Ma. *Geology* **42**, 1007–1010 (2014).
36. C. P. Chamberlain *et al*., The Cenozoic climatic and topographic evolution of the western North American Cordillera. *Am. J. Sci.* **312**, 213–262 (2012).
37. A. Mulch, Stable isotope paleoaltimetry and the evolution of landscapes and life. *Earth Planet. Sci. Lett.* **433**, 180–191 (2016).
38. K. E. Sundell, J. E. Saylor, T. J. Lapen, B. K. Horton, Implications of variable late Cenozoic surface uplift across the Peruvian Central Andes. *Sci. Rep.* **9**, 4877 (2019).
39. H. Pingel *et al*., Pliocene orographic barrier uplift in the southern Central Andes. *Geology* **42**, 691–694 (2014).
40. H. Pingel *et al*., Surface uplift and convective rainfall along the southern Central Andes (Angastaco Basin, NW Argentina). *Earth Planet. Sci. Lett.* **440**, 33–42 (2016).
41. H. Pingel *et al*., Late Cenozoic topographic evolution of the Eastern Cordillera and Puna Plateau margin in the southern Central Andes (NW Argentina). *Earth Planet. Sci. Lett.* **535**, 116112 (2020).
42. N. Kar *et al*., Paleocene-Miocene topographic and tectonic evolution of the northern Central Andean Plateau, southern Peru. *J. South Am. Earth Sci.* **121**, 104134 (2023).
43. M. R. Strecker *et al*., Tectonics and climate of the Southern Central Andes. *Annu. Rev. Earth Planet. Sci.* **35**, 747–787 (2007).
44. C. N. Garzione *et al*., Tectonic evolution of the Central Andean Plateau and implications for the growth of Plateaus. *Annu. Rev. Earth Planet. Sci.* **45**, 1–31 (2017).
45. W. Dansgaard, Stable isotopes in precipitation. *Tellus* **16**, 436–468 (1964).
46. I. Friedman, J. Gleason, A. Warden, "Ancient climate from deuterium content of water in volcanic glass" in *Climate Change in Continental Isotopic Records Monograph Series* (American Geophysical Union, 1993), vol. 78, pp. 309–319.
47. J. Quade, C. Garzione, J. Eiler, Paleoelevation reconstruction using pedogenic carbonates. *Rev. Mineral. Geochem.* **66**, 53–87 (2007).
48. A. Mulch, C. P. Chamberlain, Stable isotope paleoaltimetry in orogenic belts - The silicate record in surface and crustal geological archives. *Rev. Mineral. Geochem.* **66**, 89–118 (2007).
49. P. J. Polissar, K. H. Freeman, D. B. Rowley, F. A. McInerney, B. S. Currie, Paleoaltimetry of the Tibetan Plateau from D/H ratios of lipid biomarkers. *Earth Planet. Sci. Lett.* **287**, 64–76 (2009).
50. E. J. Cassel, D. O. Breecker, Long-term stability of hydrogen isotope ratios in hydrated volcanic glass. *Geochim. Cosmochim. Acta* **200**, 67–86 (2017).
51. B. Carrapa, P. DeCelles, P. Reiners, G. Gehrels, M. Sudo, Apatite triple dating and white mica 40Ar/39Ar thermochronology of syntectonic detritus in the Central Andes: A multiphase tectonothermal history. *Geology* **37**, 407–410 (2009).
52. M. Matteini, R. Mazzuoli, R. Omarini, R. Cas, R. Maas, Geodynamical evolution of Central Andes at 24°S as inferred by magma composition along the Calama-Olacapato-El Toro transversal volcanic belt. *J. Volcanol. Geother. Res.* **118**, 205–228 (2002).
53. J. C. M. Turner, Descripción geológica de la hoja 7c, Nevado de Cachi. Dirección Nacional de Geología y Minería (1964), p. 78.
54. M. Koukharsky, S. Quenardelle, V. D. Litvak, S. Page, E. B. Maisonnave, Plutonismo del Ordovícico inferior en el sector norte de la sierra de Macón, provincia de Salta. *Rev. Asoc. Geol. Argent.* **57**, 173–181 (2002).
55. N. Insel *et al*., Paleozoic to early Cenozoic cooling and exhumation of the basement underlying the eastern Puna Plateau margin prior to plateau growth. *Tectonics* **31**, TC6006 (2012).
56. H. Bahlburg, J. Berndt, A. Gerdes, The ages and tectonic setting of the Faja Eruptiva de la Puna Oriental, Ordovician. *NW Argentina. Lithos* **256**, 41–54 (2016).
57. P. DeCelles, B. Carrapa, G. Gehrels, Detrital zircon U-Pb ages provide provenance and chronostratigraphic information from Eocene synorogenic deposits in northwestern Argentina. *Geology* **35**, 323–326 (2007).
58. R. Pascual, Novedosos marsupiales Paleógenos de la Formacíon Pozuelos (Grupo Pastos Grandes) de la Puna, Salta, Argentina. *Ameghiniana* **20**, 265–280 (1983).
59. R. Alonso *et al*., Vertebrados Paleógenos de la Puna Austral: Sus aportes a la evolucíon biogeográfica. *Abst. V J. Argent. Paleontol. Vertebrados* **6** (1988).
60. F. J. Goin, A. Candela, G. López, Middle Eocene marsupials from Antofagasta de la Sierra, Northwestern Argentina. *Geobios* **31**, 75–85 (1998).
61. C. del Papa *et al*., Sedimentological, geochemical and paleontological insights applied to continental omission surfaces: A new approach for reconstructing an Eocene foreland basin in NW Argentina. *J. South Am. Earth Sci.* **29**, 327–345 (2010).
62. J. Babot, D. García-López, V. Deraco, C. M. Herrera, C. del Papa, Mamíferos Paleógenos del subtrópico de Argentina: Síntesis de estudios estratigráficos, cronológicos y taxonómicos *Ciencias de la Tierra y Recursos Naturales del NOA, Relatorio del XX Congreso Geológico Argentino*, pp. 730–753 (2017).
63. C. Montero-López, C. del Papa, F. Hongn, M. R. Strecker, A. Aramayo, Synsedimentary broken-foreland tectonics during the Paleogene in the Andes of NW Argentine: New evidence from regional to centimetre-scale deformation features. *Basin Res.* **30**, 142–159 (2018).
64. F. Hongn *et al*., "Fragmented Paleogene foreland basin in the Valles Calchaquíes, NW of Argentina" in *Cenozoic Geology of the Central Andes of Argentina*, S. Salfity, R. A. Marquillas, Eds. (SCS Publisher, 2011), pp. 189–209.
65. D. S. Vandervoort, *Non-Marine Evaporite Basin Studies, Southern Puna Plateau, Central Andes* (Cornell University, Ithaca, USA, 1993).
66. R. Marrett, R. Allmendinger, R. Alonso, R. Drake, Late Cenozoic tectonic evolution of the Puna Plateau and adjacent foreland, northwestern Argentine Andes. *J. South Am. Earth Sci.* **7**, 179–207 (1994).
67. R. Alonso, *Ocurrencia, posición estratigráfica y génesis de los depósitos de boratos de la Puna argentina* (Universidad Nacional de Salta, Salta, Argentina, 1986).
68. E. Donato, Características estructurales del sector occidental de la Puna salteña. *Bol Inv Petrol* **12**, 89–99 (1987).
69. D. S. Vandervoort, Stratigraphic response to saline lake-level fluctuations and the origin of cyclic nonmarine evaporite deposits: The Pleistocene Blanca Lila Formation, northwest Argentina. *GSA Bull.* **109**, 210–224 (1997).

70. R. R. Canavan *et al*., Early Cenozoic uplift of the Puna Plateau, Central Andes, based on stable isotope paleoaltimetry of hydrated volcanic glass. *Geology* **42**, 447–450 (2014).
71. B. Bekeschus *et al*., Palaeoclimate reconstructions from lacustrine terraces and lake-balance modeling in the southern Central Andes: New insights from Salar de Pocitos (Salta Province, Argentina). *Geophys. Res. Abst.* **15**, EGU2013-7853 (2013).
72. L. V. Luna *et al*., Glacial chronology and production rate cross-calibration of five cosmogenic nuclide and mineral systems from the southern Central Andean Plateau. *Earth Planet. Sci. Lett.* **500**, 242–253 (2018).
73. T. Cladouhos, R. Allmendinger, B. Coira, E. Farrar, Late Cenozoic deformation in the Central Andes: Fault kinematics from the northern Puna, northwestern Argentina and southwestern Bolivia. *J. South Am. Earth Sci.* **7**, 209–228 (1994).
74. L. M. Schoenbohm, M. R. Strecker, Normal faulting along the southern margin of the Puna Plateau, northwest Argentina. *Tectonics* **28** (2009).
75. A. Rohrmann *et al*., Can stable isotopes ride out the storms? The role of convection for water isotopes in models, records, and paleoaltimetry studies in the Central Andes. *Earth Planet. Sci. Lett.* **407**, 187–195 (2014).
76. R. P. Fiorella, C. J. Poulsen, R. S. P. Zolá, M. L. Jeffery, T. A. Ehlers, Modern and long-term evaporation of Central Andes surface waters suggests paleo archives underestimate Neogene elevations. *Earth Planet. Sci. Lett.* **432**, 59–72 (2015).
77. J. Bershaw, J. E. Saylor, C. N. Garzione, A. Leier, K. E. Sundell, Stable isotope variations ($\delta$18O and $\delta$D) in modern waters across the Andean Plateau. *Geochim. Cosmochim. Acta* **194**, 310–324 (2016).
78. D. S. Vandervoort, T. E. Jordan, P. K. Zeitler, R. N. Alonso, Chronology of internal drainage development and uplift, southern Puna Plateau, Argentine central Andes. *Geology* **23**, 145–148 (1995).
79. M. A. Reguero, D. C. Croft, G. M. López, R. N. Alonso, Eocene archaeohyracids (Mammalia: Notoungulata: Hegetotheria) from the Puna, northwest Argentina. *J. South Am. Earth Sci.* **26**, 225–233 (2008).
80. D. A. Garcia-Lopez, M. J. Babot, Notoungulate faunas of north-western Argentina: New findings of early-diverging forms from the Eocene Geste Formation. *J. Syst. Palaeontol.* **13**, 557–579 (2014).
81. M. S. de la Fuente *et al*., A new podocnemidid (Pleurodira: Pelomedusoides) from the Eocene of north-western Argentina, with comments on its evolutionary relationships and palaeoenvironmental settings. *J. Syst. Palaeontol.* **20**, 2081939 (2022).
82. S. Jimenez-Rodriguez, M. Dettinger, J. Quade, K. E. Murray, Paleoaltimetry of the Western Andes in Northern Chile ( 18.5–19.5°S). *Am. J. Sci.* **321**, 491–533 (2021).
83. B. Carrapa, P. G. DeCelles, "Regional exhumation and kinematic history of the central Andes in response to cyclical orogenic processes" in *Geodynamics of a Cordilleran Orogenic System: The Central Andes of Argentina and Northern Chile*, P. DeCelles, M. N. Ducea, B. Carrapa, P. Kapp, Eds. (Geological Society of America, 2015).
84. P. Reiners *et al*., "Low-temperature thermochronologic trends across the central Andes, 21°S-28°S" in *Geodynamics of a Cordilleran Orogenic System: The Central Andes of Argentina and Northern Chile*, P. G. DeCelles, M. N. Ducea, B. Carrapa, P. A. Kapp, Eds. (Geological Society of America, 2015).
85. B. Carrapa, P. G. DeCelles, Eocene exhumation and basin development in the Puna of northwestern Argentina. *Tectonics* **27**, TC1015 (2008).
86. F. Hongn *et al*., Middle Eocene deformation and sedimentation in the Puna-Eastern Cordillera transition (23°–26°S): Control by preexisting heterogeneities on the pattern of initial Andean shortening. *Geology* **35**, 271–274 (2007).
87. C. Montero-López, P. Ballato, A. Aramayo, "New evidences of the Paleogene and Early Miocene unconformity in the Quebrada de Carachi, El Toro basin, Cordillera Oriental (NW Argentina)" in *Actas del XX Congreso Geológico Argentino* (San Miguel de Tucumán, Argentina, 2017), pp. 117–118.
88. E. O. Zappettini, G. Blasco, Hoja Geológica 2569-II, Socompa, Provincia de Salta. *Boletín del Inst. Geol. Rec. Miner. Ser. Geol. Minero Argent.* **260**, 1–62 (2001).
89. L. M. Schoenbohm, B. Carrapa, "Miocene-Pliocene shortening, extension, and mafic magmatism support small-scale lithospheric foundering in the central Andes, NW Argentina" in *Geodynamics of a Cordilleran Orogenic System: The Central Andes of Argentina and Northern Chile*, P. DeCelles, M. N. Ducea, B. Carrapa, P. Kapp, Eds. (Geological Society of America, 2015).
90. M. R. Strecker, *Late Cenozoic landscape development, the Santa María Valley, Northwest Argentina* (Cornell University, Ithaca, USA, 1987).
91. J. Andersen, O. H. Gogus, R. N. Pysklywec, T. Santimano, E. S. Uluocak, Symptomatic lithospheric drips triggering fast topographic rise and crustal deformation in the Central Andes. *Commun. Earth Environ.* **3**, 150 (2022).
92. C. del Papa *et al*., Middle Eocene-Oligocene broken-foreland evolution in the Andean Calchaqui Valley, NW Argentina: Insights from stratigraphic, structural and provenance studies. *Basin Res.* **25**, 574–593 (2013).
93. A. Deeken *et al*., Development of the southern Eastern Cordillera, NW Argentina, constrained by apatite fission track thermochronology: From early Cretaceous extension to middle Miocene shortening. *Tectonics* **25**, TC6003 (2006).
94. H. Ege, E. R. Sobel, E. Scheuber, V. Jacobshagen, Exhumation history of the southern Altiplano Plateau (southern Bolivia) constrained by apatite fission track thermochronology. *Tectonics* **26**, TC1004 (2007).
95. D. M. Pearson *et al*., Major Miocene exhumation by fault-propagation folding within a metamorphosed, early Paleozoic thrust belt: Northwestern Argentina. *Tectonics* **31**, TC4023 (2012).
96. C. I. Galli *et al*., Tectonic controls on the evolution of the Andean Cenozoic foreland basin: Evidence from fluvial system variations in the Payogastilla Group, in the Calchaquí, Tonco and Amblayo Valleys, NW Argentina. *J. South Am. Earth Sci.* **52**, 234–259 (2014).
97. R. Zhou, L. M. Schoenbohm, E. R. Sobel, D. W. Davis, J. Glodny, New constraints on orogenic models of the southern Central Andean Plateau: Cenozoic basin evolution and bedrock exhumation. *GSA Bull.* **129**, 152–170 (2017).
98. C. N. Garzione *et al*., Clumped isotope evidence for diachronous surface cooling of the Altiplano and pulsed surface uplift of the Central Andes. *Earth Planet. Sci. Lett.* **393**, 173–181 (2014).
99. T. E. Jordan *et al*., Uplift of the Altiplano-Puna Plateau: A view from the west. *Tectonics* **29**, TC5007 (2010).
100. H. Pingel *et al*., KMZ dataset - Miocene surface uplift and orogenic evolution of the southern Andean Plateau (central Puna), northwestern Argentina, 2023. https://figshare.com/articles/dataset/Kmz_file/24076044, 10.6084/m9.figshare.24076044.v1, 1 September 2023.